Letter

Emergence of pseudoresonance in high-intensity resonant inelastic x-ray scattering

```
Sang-Kil Son (손상길), 1,*,† Thomas M. Baumann, 2,*,‡ Jacob Pedersen, 3,4 Laura Budewig, 1,5 Kai Li,6,7 Hans Ågren, 8
   Olle Biörneholm . Rebecca Boll . John Bozek . Carl Caleman . Sebastian Cardoch . Lucas M. Cornetta .
Alberto De Fanis , <sup>2</sup> Emiliano De Santis , <sup>11,8</sup> Simon Dold , <sup>2</sup> Gilles Doumy , <sup>7</sup> Ulrich Eichmann , <sup>12</sup> Xiaochun Gong , <sup>13</sup> Johan Gråsjö , <sup>14,8</sup> Alice E. Green , <sup>15,16,2</sup> Iyas Ismail , <sup>17</sup> Ludvig Kjellsson , <sup>18</sup> Eva Lindroth , <sup>19</sup> Tommaso Mazza , <sup>2</sup> Jacobo Montaño, <sup>2</sup> Terry Mullins , <sup>1</sup> Christian Ott , <sup>20</sup> Yevheniy Ovcharenko , <sup>2</sup> Thomas Pfeifer , <sup>20</sup> Maria Novella Piancastelli , <sup>17</sup> Ralph Püttner , <sup>21</sup> Nils Rennhack , <sup>2</sup> Nina Rohringer , <sup>15</sup> Cecilia Sánchez-Hanke , <sup>22</sup>
     Conny Såthe , <sup>18</sup> Philipp Schmidt , <sup>2</sup> Björn Senfftleben , <sup>2</sup> Marc Simon , <sup>17</sup> Nicuşor Tîmneanu , <sup>8</sup> Moto Togawa , <sup>2</sup>
     Kiyoshi Ueda, <sup>23,24</sup> Sergey Usenko <sup>10</sup>, <sup>2</sup> Hans Jakob Wörner <sup>10</sup>, <sup>25</sup> Weiqing Xu <sup>10</sup>, <sup>26,27</sup> Zhong Yin <sup>10</sup>, <sup>28</sup> Linda Young <sup>10</sup>, <sup>6,7</sup>
                Joseph Nordgren , <sup>8</sup> Marcus Agåker , <sup>18,8</sup> Johan Söderström , <sup>8</sup> Sonia Coriani , <sup>3</sup> Michael Meyer , <sup>2</sup>
                                                       Robin Santra, 1,5 and Jan-Erik Rubensson, 8,8
                  <sup>1</sup>Center for Free-Electron Laser Science CFEL, Deutsches Elektronen-Synchrotron DESY, Hamburg, Germany
                                                                <sup>2</sup>European XFEL, Schenefeld, Germany
                                      <sup>3</sup>Department of Chemistry, Technical University of Denmark, Lyngby, Denmark
                          <sup>4</sup>Department of Chemistry, Norwegian University of Science and Technology, Trondheim, Norway
                                             <sup>5</sup>Department of Physics, University of Hamburg, Hamburg, Germany
                                         <sup>6</sup>Department of Physics, The University of Chicago, Chicago, Illinois, USA
                         <sup>7</sup>Chemical Sciences and Engineering Division, Argonne National Laboratory, Lemont, Illinois, USA
                                       <sup>8</sup>Department of Physics and Astronomy, Uppsala University, Uppsala, Sweden
                                                        <sup>9</sup>Synchrotron SOLEIL, Gif-sur-Yvette Cedex, France
                                             <sup>10</sup>Instituto de Física da Universidade de São Paulo, São Paulo, Brazil
                                     <sup>11</sup>Department of Physics, University of Rome Tor Vergata and INFN, Roma, Italy
                                                                 <sup>12</sup>Max-Born-Institut, Berlin, Germany
                  <sup>13</sup>State Key Laboratory of Extreme Photonics and Instrumentation, College of Optical Science and Engineering,
                                                                Zhejiang University, Hangzhou, China
                                        <sup>14</sup>Department of Medicinal Chemistry, Uppsala University, Uppsala, Sweden
                                                     <sup>15</sup>Stanford PULSE Institute, Menlo Park, California, USA
                                <sup>16</sup>EaStCHEM School of Chemistry, University of Edinburgh, Edinburgh, United Kingdom
                      <sup>17</sup>Laboratoire de Chimie Physique - Matière et Rayonnement, CNRS, Sorbonne Université, Paris, France
                                                      <sup>18</sup>MAX IV Laboratory, Lund University, Lund, Sweden
                                              <sup>19</sup>Department of Physics, Stockholm University, Stockholm, Sweden
                                                   <sup>20</sup>Max-Planck-Institut für Kernphysik, Heidelberg, Germany
                                                <sup>21</sup> Fachbereich Physik, Freie Universität Berlin, Berlin, Germany
                                                         <sup>22</sup>Diamond Light Source, Didcot, United Kingdom
                                                  <sup>23</sup>Department of Chemistry, Tohoku University, Sendai, Japan
                                  <sup>24</sup>School Physical Science and Technology, ShanghaiTech University, Shanghai, China
                                            <sup>25</sup>Laboratory of Physical Chemistry, ETH Zürich, Zurich, Switzerland
                                     <sup>26</sup>Center for Transformative Science, ShanghaiTech University, Shanghai, China
             <sup>27</sup>Shanghai HIgh repetitioN rate XFEL and Extreme light facility (SHINE), ShanghaiTech University, Shanghai, China
                        <sup>28</sup>International Center for Synchrotron Radiation Innovation Smart, Tohoku University, Sendai, Japan
```

(Received 18 June 2025; accepted 1 October 2025; published 7 November 2025)

We report resonant inelastic x-ray scattering (RIXS) spectra of neon atoms interacting with intense x-ray pulses generated using an x-ray free-electron laser (XFEL). We find that an unexpected peak emerges near the $K\alpha$ line of Ne, which does not coincide with any physical resonances of neon ions. We perform theoretical calculations based on a quantum-state-resolved rate-equation approach with x-ray-induced processes including

Published by the American Physical Society under the terms of the Creative Commons Attribution 4.0 International license. Further distribution of this work must maintain attribution to the author(s) and the published article's title, journal citation, and DOI.

^{*}These authors contributed equally to this work.

[†]Contact author: sangkil.son@cfel.de

[‡]Contact author: thomas.baumann@xfel.eu

[§]Contact author: jan-erik.rubensson@physics.uu.se

possible resonant excitations. Our dynamics simulations demonstrate that a sequence of multiple resonant photoabsorption events are involved and the interplay of those multiple resonances in combination with the relatively large spectral bandwidth of XFEL radiation leads to the emergent resonance-like structure at a position where no resonances exist. Our finding offers critical guidance for future applications of high-intensity RIXS at XFEL facilities.

DOI: 10.1103/drmh-vmgk

X-ray multiphoton physics [1], which occurs when matter interacts with an intense x-ray pulse, has been studied mainly by measuring yields of ion charge states long after the x-ray pulse is over [2–13]. In addition to electron spectra [2,4,14–17], photon spectra can provide information on transient intermediate states formed during the interaction with the x-ray pulse [7,18–21]. In principle, x-ray emission spectra can also provide electronic-quantum-state specific information on ionization dynamics, which is not directly available via charge-state measurements. However, this has been limited so far because of a lack of high-resolution spectrometers at x-ray free-electron laser (XFEL) facilities.

Resonant inelastic x-ray scattering (RIXS) [22] is a major method for investigating electronic structure and dynamics, with applications ranging from basic atomic physics to materials science. The remarkable properties of XFEL beams, namely, the extremely high peak intensity and the ultrafast pulse duration [23,24], have broadened the scope of RIXS toward time-resolved RIXS [25] and nonlinear RIXS [26] including stimulated x-ray Raman scattering [27–30] and x-ray four-wave mixing [31,32]. Because of the small yield of the RIXS signal, it is also desirable to utilize higher x-ray fluences available from XFELs [33–38].

When pursuing high-intensity RIXS, however, multiple resonances are hit one after the other and then the ionization dynamics are dramatically altered in the course of x-ray multiphoton absorption. One prominent example is resonance-enabled (or -enhanced) x-ray multiple ionization [7,10,39–41]. When multiple resonances are involved in the RIXS process, the Kramers-Heisenberg formula (to leading order in perturbation theory, only one photon is absorbed and only one photon is emitted) is no longer applicable. Instead, it is inevitable to consider multi-photon-in and multi-photon-out or, at least, multi-photon-in and one-photon-out processes, which we refer to as multi-RIXS [42]. In the multi-photon-in picture, the last excitation step in the multi-RIXS process happens not from the ground state, but from an excited state resulting from previous resonant excitations.

Another aspect in RIXS with XFELs is the relatively large spectral bandwidth of XFEL radiation due to the self-amplified spontaneous emission (SASE) process [23], which spectrally covers about 1% of the photon energy. A typical way to achieve better spectral resolution is to reduce the bandwidth by using a monochromator [37,43], but this leads to a considerable reduction of the x-ray fluence by more than two orders of magnitude [44], thereby sacrificing the potential advantage, in terms of RIXS signal strength, that using the full XFEL fluence might offer.

Here, we present a joint experimental and theoretical study of multi-RIXS spectroscopy of neon atoms with ultraintense x-ray pulses generated by the European XFEL [45]. We demonstrate how the interplay of multiple resonant photoabsorption events in combination with the relatively large spectral bandwidth of nonmonochromatized XFEL radiation may lead to the emergence of pseudoresonance structures, at spectral positions at which no actual resonances exist. This indicates that XFEL-based x-ray absorption spectroscopy in combination with x-ray emission spectroscopy requires careful interpretation.

We measured multi-RIXS spectra by using the onedimensional (1D) imaging soft x-ray spectrometer [46] installed at the Small Quantum Systems (SQS) scientific instrument [47] of the European XFEL. The neon target was prepared in a gas cell at an estimated pressure of 0.14 bar. The incoming XFEL photon energy was varied from 852 eV to 881 eV, facilitated by the variable-gap undulators available at the European XFEL. The XFEL photon energy was calibrated with an estimated accuracy of $\pm 1.2 \, \text{eV}$ and the spectral bandwidth was estimated to be 1.2% full width at half maximum (FWHM) using known transitions of neutral Ne atom (see Sec. A and Fig. S1 in the Supplemental Material [48] for the detailed calibration procedure). The outgoing x-ray photons were detected with a spectrometer resolution of around 0.3 eV in the energy range of $844-860 \,\mathrm{eV}$, which covers the $K\alpha$ fluorescence energies of neon charge states up to +2.

Figure 1 shows a two-dimensional color map of measured multi-RIXS spectra of neon. On the one hand, the x-ray emission energy (fluorescence energy, $E_{\rm F}$, on the x axis) carries information on the core-excited states that the fluorescence comes from. The strong vertical line at $E_{\rm F}=849\,{\rm eV}$ is assigned to the $K\alpha$ line of Ne⁺1s⁻¹. The weaker peak around $E_{\rm F}=855\,{\rm eV}$ corresponds to the ion-core charge ($Q_{\rm ic}$) of +2,

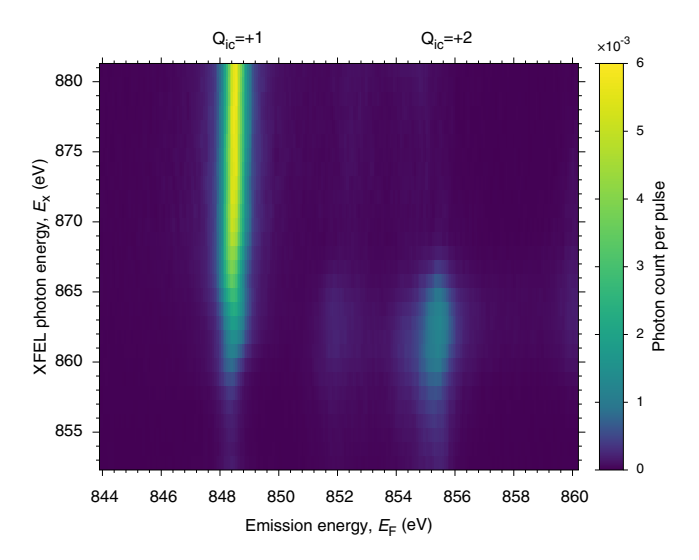


FIG. 1. Measured multi-RIXS spectra of neon as a function of the x-ray emission energy and of the incident XFEL photon energy.

TABLE I. Transition energies (in eV) involved in the present work. A longer version, which includes more transitions and also shows oscillator strengths, can be found in Table S1 in the Supplemental Material [48]. The electron configurations ($\ell=s$ or p) are given for lower and upper states, and [Ne] indicates the neutral neon. Q and $Q_{\rm ic}$ are the atomic charge and the ion-core charge of the lower state, respectively.

Trans.	Q	$Q_{ m ic}$	Lower	Upper	$E_{ m trans}$
1 <i>s</i> -2 <i>p</i>	+0	+1	$2p^{-1}3p$	$1s^{-1}3p$	848 ^a
	+1	+1	$2p^{-1}$	$1s^{-1}$	849 ^b
	+1	+2	$2p^{-1}2\ell^{-1}3p$	$1s^{-1}2\ell^{-1}3p$	852–856 ^a
	+2	+2	$2p^{-1}2\ell^{-1}$	$1s^{-1}2\ell^{-1}$	851-856 ^b
	+3	+3	$2p^{-1}2\ell^{-2}$	$1s^{-1}2\ell^{-2}$	861-862 ^c
1s- $3p$	+0	+0	[Ne]	$1s^{-1}3p$	867 ^d

^aPresent calculations.

where Q_{ic} is defined by the nuclear charge minus the total number of electrons in the initially occupied subshells (1s, 2s,and 2p). For analyzing fluorescence spectra, Q_{ic} is more useful than Q, because E_F is mainly dependent on Q_{ic} , as shown in Table I. On the other hand, the incident XFEL photon energy (excitation energy, E_x , on the y axis) provides information on how the fluorescing atomic states are generated. For the standard $K\alpha$ line, the core-hole state $1s^{-1}$ is created by 1s photoionization when E_x is higher than the 1s ionization threshold $(\sim 870 \,\mathrm{eV})$. This is not a resonance feature, thus giving rise to an extended vertical structure for $E_x > 870 \,\mathrm{eV}$. At lower E_x , resonant $1s \to np$ excitation $(n \ge 3)$ happens, resulting in core-excited $1s^{-1}np$ states, which yield slightly lower $E_{\rm F}$ than $1s^{-1}$ [52]. Those resonances may be expected to lead to a series of peaks at the associated resonance energies. However, the signals of $1s^{-1}$ and $1s^{-1}np$ form a quasicontinuum starting at ~860 eV in Fig. 1 because of the relatively large XFEL bandwidth (\sim 10 eV).

Let us examine the fluorescence signal for $Q_{ic} = +2$, which shows a resonance feature at $E_{\rm x} \sim 862\,{\rm eV}$ and $E_{\rm F} \sim$ 855 eV. To this end, we list in Table I 1s-2p and 1s-3ptransition energies relevant to the present work. These are either taken from the literature [20,49–51] or calculated using multistate restricted active space second-order perturbation theory (MS-RASPT2) [53-56] with OPENMOLCAS [57] (see Sec. B in the Supplemental Material [48]). As is evident from Table I, the upper states that give rise to x-ray emission near 855 eV have the ion-core configuration $1s^{-1}2\ell^{-1}$ ($\ell = s$ or p), with or without an np spectator. However, which of the transitions could potentially explain the resonance seen in Fig. 1, with respect to the XFEL photon energy? None of those for $Q \leq +2$ that lie close to the resonance peak position of $861.8 \pm 1.2 \,\mathrm{eV}$ happen to actually coincide with that peak position: They all are below ($\leq 855 \, \text{eV}$) or above (867 eV) by several eV. (The uncertainty in the peak position reflects the accuracy of the XFEL photon-energy calibration).

An exception is the 1s-2p transition for Q=+3, but this charge state would have to be converted back into Q=+2 before x-ray emission takes place. In this scenario, the short-lived Ne³+1s-¹ 2ℓ -², produced via resonant excitation of Ne³+2p-¹ 2ℓ -² near 862 eV, would have to recombine with a free electron to form Ne²+1s-¹ 2ℓ -¹ to produce x-ray emission near 855 eV. This pathway is strongly suppressed because the time scale for recombination is much longer than the lifetime of core-excited Ne³+ (~3 fs). Moreover, the fluorescence signal from core-excited Ne³+ itself (i.e., before any potential electron recombination with Ne³+) is about 1.7 times weaker than that for $Q_{ic} = +2$ in our measurement. Therefore, under the experimental conditions underlying the present work, it is very unlikely that electron recombination into the L shell of core-excited Ne³+ provided a significant pathway to $Q_{ic} = +2$ fluorescence.

So far we have been considering one-photon-one-electrontype transitions, as listed in Table I. Another potential candidate for resonant photoabsorption near 862 eV is onephoton double excitation, for instance, $2s^{-1} \rightarrow 1s^{-1}2p^{-1}3\ell$ $(\ell = s \text{ or } d)$, which also gives rise to x-ray emission near 855 eV. Our MS-RASPT2 calculations, however, indicate that the associated oscillator strength is about two orders of magnitude smaller than that for a typical one-photon 1s-2psingle excitation (see Table S2 in the Supplemental Material [48]). Therefore, we rule out one-photon double excitation as a potential explanation of the resonance feature. Hence, the question still remains: Which transitions can eventually form the ion-core configuration $1s^{-1}2\ell^{-1}$ ($Q_{ic}=+2$), and how come we observe resonantly enhanced fluorescence from $Q_{\rm ic} = +2$ at an XFEL photon energy that does not match any resonances for $Q \leq +2$?

To resolve this mystery, we performed dynamics simulations on neon using XATOM [58], which has been extended to handle quantum-state-resolved ionization and resonance dynamics [59,60] via a Monte Carlo on-the-fly rate-equation approach [8]. State-to-state cross sections and rates of photoionization, resonant excitation, Auger-Meitner decay, and spontaneous emission were calculated and included in the rate-equation matrix. In addition, shakeoff processes [61,62] were taken into account in an ad hoc manner (see Sec. C in the Supplemental Material [48]). For transition energies involved in the standard $K\alpha$ line, we employed experimental data [49,51]. All other transition energies were calculated using XATOM, which were found comparable with MS-RASPT2 results (see Table S1 in the Supplemental Material [48]).

Regarding XFEL pulse parameters in the calculations, the pulse duration was fixed at 10 fs FWHM. Eleven different fluence points from $1\times 10^9\,\mathrm{photons/\mu m^2}$ to $1\times 10^{12}\,\mathrm{photons/\mu m^2}$ were considered and then the theoretical results were volume-integrated [63,64]. We employed a peak fluence of $1\times 10^{11}\,\mathrm{photons/\mu m^2}$, according to the best fit of the quasicontinuum shape of the measured $K\alpha$ line (see Sec. A in the Supplemental Material [48] for details). For each x-ray parameter set, we calculated more than 200 000 Monte Carlo trajectories through the space of quantum states of neon charge states up to +3, including all possible excitations into (n,ℓ) subshells with $n\leqslant 7$ and $\ell=s,p,$ and d.

In Fig. 2, we compare our calculated x-ray absorption spectra with experimental results obtained from Fig. 1. The experiment plot in Fig. 2(a) shows fluorescence counts after integrating signals for $Q_{\rm ic}=+1$ ($E_{\rm F}<850\,{\rm eV}$) and +2 ($850\,{\rm eV}\leqslant E_{\rm F}\leqslant858\,{\rm eV}$), respectively. After integration, the

^bReference [49].

^cReference [20].

dReferences [50,51].

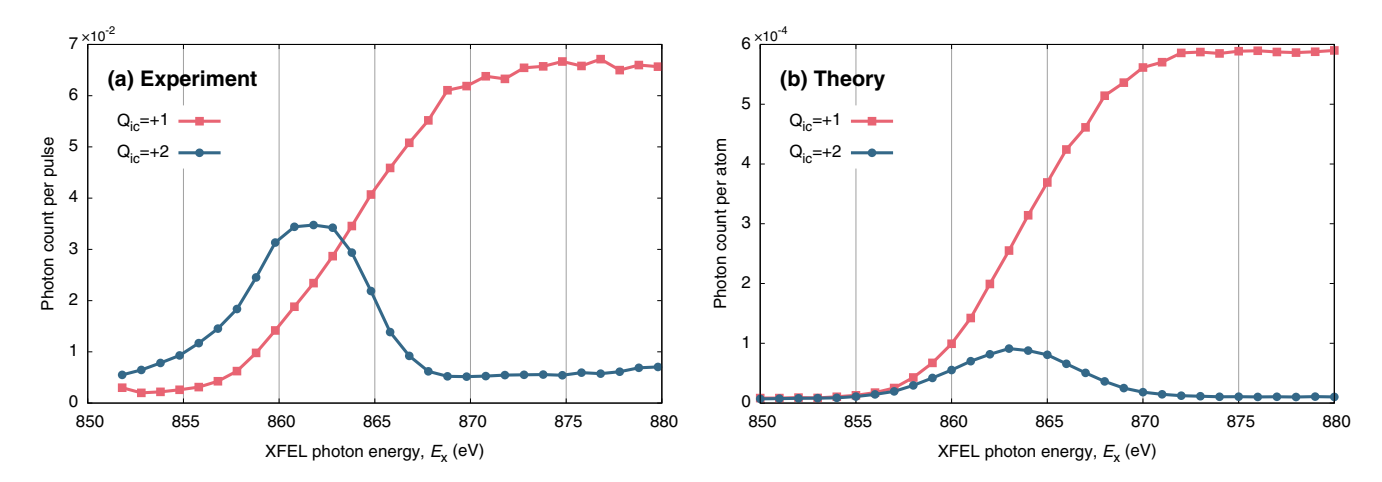


FIG. 2. (a) Experimental and (b) theoretical fluorescence counts for the ion-core charges of +1 and +2. The known resonances are located at $E_x = 851-856 \,\text{eV}$ ($1s \rightarrow 2p$ excitation at $Q_{ic} = +2$) and $E_x = 867 \,\text{eV}$ ($1s \rightarrow 3p$ excitation at $Q_{ic} = +0$).

height of $Q_{\rm ic}=+2$ is almost half of that of $Q_{\rm ic}=+1$. The peak position of +2 is located at $E_{\rm x}\sim 862\,{\rm eV}$ and, as mentioned earlier, does not coincide with any of the resonances in Table I; neither in the range $851-856\,{\rm eV}$ nor at $867\,{\rm eV}$ can any peaks be discerned, within the accuracy of the XFEL photonenergy calibration. The linewidth is $7.5\,{\rm eV}$ FWHM, which is narrower than the estimated XFEL bandwidth ($\sim 10\,{\rm eV}$ FWHM). The theory data in Fig. 2(b) are in good agreement with the experimental data: They clearly demonstrate the existence of a resonance-like feature where none would be expected (recall that our calculations employed the transition energies listed in Table I).

To identify the mechanisms giving rise to fluorescence at $Q_{\rm ic} = +2$, we analyze the Monte Carlo trajectories that pass through the corresponding core-excited states in the left panel of Fig. 3. In fact, there are many different ionization and resonance pathways to reach the ion-core charge of +2, as sketched in the right panel of Fig. 3. For example, when the XFEL photon energy is higher than the ionization threshold of

neutral Ne, the dominant mechanism leading to fluorescence at +2 is one core photoionization (P) and subsequently one valence photoionization (V), plotted in dark green. At lower photon energies, one valence photoionization accompanied by shakeoff (SO) generates $Ne^{2+}2p^{-2}$, which undergoes resonant $1s \rightarrow 2p$ excitation (R_{2p}) and produces fluorescence (F). This pathway is shown in light blue. However, in the vicinity of the $Q_{ic} = +2$ peak, the dominant pathway, $R_{np}-A-R_{2p}-F$ (orange), involves two resonant photoabsorption events, $1s \rightarrow$ np and $1s \rightarrow 2p$, and an intermediate Auger-Meitner decay (A). The last two steps in this pathway, R_{2p} -F, represent resonant x-ray emission of Ne⁺2 $p^{-2}np$ (mainly, n = 3), which gives an elastic contribution at $E_{\rm x} = E_{\rm F} \sim 855\,{\rm eV}$. The first two steps, R_{np} —A, represent the resonant Auger-Meitner process of neutral Ne, with resonant $1s \rightarrow np$ excitation at $E_x =$ 867 eV or higher.

In our calculations, each resonance is described by a Gaussian spectral profile [60], resulting from convolving the resonant-excitation cross section with a Gaussian

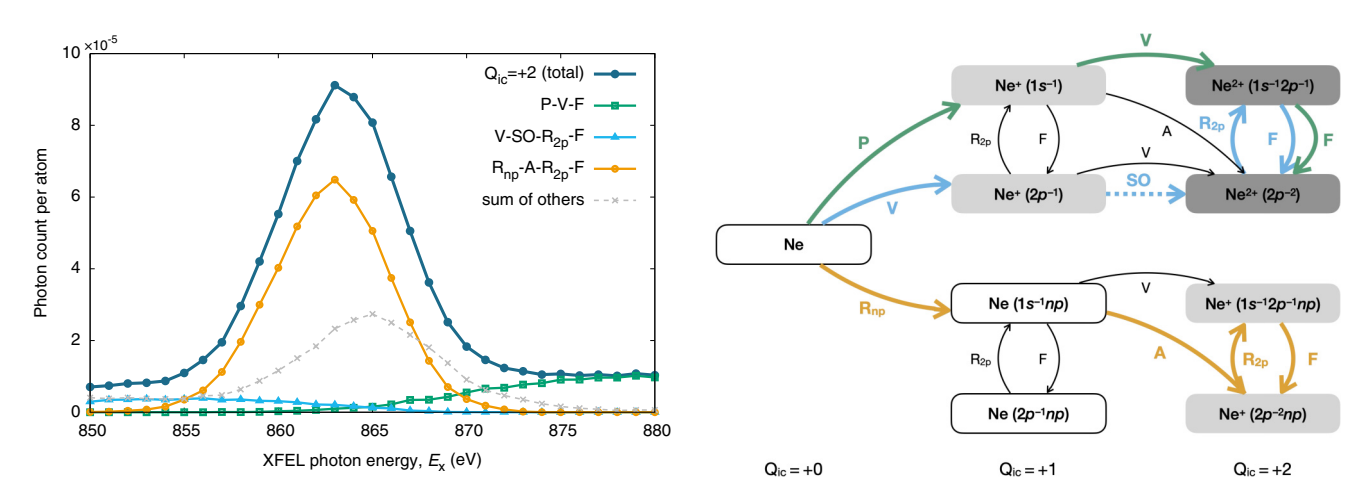


FIG. 3. Ionization and resonance mechanisms leading to fluorescence at the ion-core charge of +2. Left panel: Decomposition of the resonance-like feature. The dark blue line indicates the total counts for $Q_{ic} = +2$. Contributions to the total are plotted with different colors (orange, dark green, light blue, and gray). Right panel: Pathways for producing fluorescence up to Ne^{2+} . Individual ion-core charges are aligned in different columns. The white boxes refer to neutral Ne, the light gray ones to Ne^{+} , and the dark gray ones to Ne^{2+} . Configurations with $2s^{-1}$ are not included for brevity. P: core photoionization; V: valence photoionization; R_{np} : resonant $1s \rightarrow np$ photoexcitation; A: Auger-Meitner decay; F: fluorescence; and SO: shakeoff.

approximating the experimental XFEL spectral distribution obtained after averaging over many XFEL pulses. The result of the convolution may be approximated by a pure Gaussian because the natural linewidth of a core-excited state of neon (typically $\sim 0.3 \, \text{eV}$) is much narrower than the XFEL bandwidth ($\sim 10 \, \text{eV}$ FWHM).

For the dominant $R_{np}-A-R_{2p}-F$ pathway, this has the following important consequence. The $R_{2p}-F$ process, with a Gaussian absorption profile centered at $E_x \sim 855 \, \mathrm{eV}$, is conditioned on the $R_{np}-A$ process, with a Gaussian absorption profile centered at $E_x \sim 867 \, \mathrm{eV}$ (for n=3), taking place first. Hence, the fluorescence probability for this pathway depends on the product of the $R_{np}-A$ probability and the probability for the $R_{2p}-F$ process in the states populated via $R_{np}-A$. In other words, the dependence of the fluorescence yield on the XFEL photon energy is given by the product of the Gaussian profiles of the R_{np} and R_{2p} transitions.

This is the key to understanding why in Fig. 1 there is a resonance-like feature at a position where no resonant transitions exist: The product of two Gaussians is a single Gaussian, centered at the midpoint between the two original Gaussians, if their widths are identical (see Sec. D in the Supplemental Material [48]). Therefore, the individual R_{np} and R_{2p} resonances are not visible, but instead a new resonance-like structure, which we call a pseudoresonance, emerges. Given the energies of the R_{np} and R_{2p} transitions, the pseudoresonance would be expected to be centered at around 861 eV or higher. The linewidth of the pseudoresonance is given by the given Gaussian width times $1/\sqrt{2}$. Both position and linewidth coincide with what are observed experimentally.

Although the overall pseudoresonance structure observed in experiment is well reproduced by theory in Fig. 2, there are quantitative discrepancies. The height of the theoretical +2peak, relative to the +1 counts, is lower than in experiment, while the peak position is shifted to higher photon energy by \sim 1 eV, which, however, we consider negligible to within the accuracy of the experimental peak position. Also the FWHM in theory (8.0 eV) is somewhat larger than in experiment (7.5 eV). These discrepancies are, at least in part, due to the incomplete characterization of the XFEL beam, which would affect the relative contributions of individual pathways. We numerically found that a higher fluence nonlinearly boosts the whole +2 yields, because they are produced mainly by two-photon absorption. We also found that a longer pulse duration produces a higher peak height, because it facilitates the A process in R_{np} -A- R_{2p} -F, similar to the frustrated absorption phenomenon [2,3]. (Further discussion of the impact of the XFEL beam parameters may be found in Sec. E in the Supplemental Material [48].)

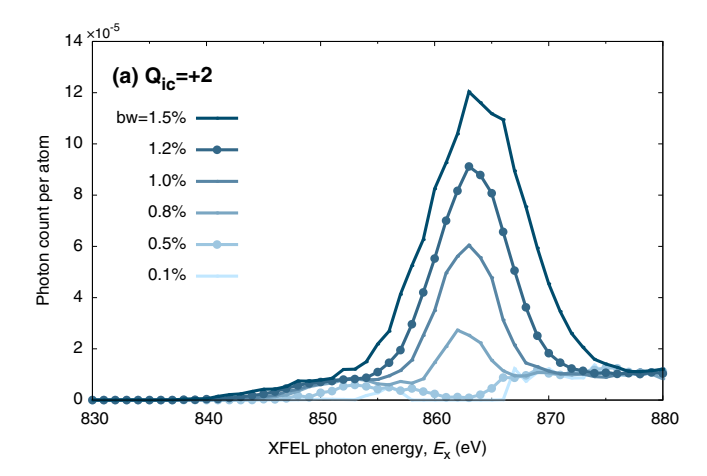
Moreover, we considered the possibility that the target gas contained, in addition to neutral Ne atoms, Ne⁺ ions generated in earlier XFEL pulses. The presence of Ne⁺ would have contributed to more +2 signal via one resonance only, at \sim 855 eV. We numerically found that, when the ionization dynamics start from Ne⁺, both +1 and +2 signals are strongly enhanced at lower XFEL photon energy, which does not match the experimental results in Fig. 2(a) (see Sec. F in the Supplemental Material [48]).

Since, at the peak fluence applied here, we expect partial saturation of R_{np} (see Sec. A in the Supplemental Mate-

rial [48]), R_{2p} should be even more strongly saturated. This would cause the effective linewidth for R_{2p} to be larger than that for R_{np} . With such unequal linewidths, the resulting pseudoresonance is then shifted toward R_{np} , depending on the fluence (see Sec. D in the Supplemental Material [48]). This could be the reason why both experimental and theoretical peak positions are a bit higher than the midpoint between R_{2p} and R_{np} . Note, however, that we calibrated the XFEL photon energy and fluence distribution hand in hand. Therefore, to convincingly demonstrate the impact of saturation on the experimental peak position of the pseudoresonance, one would have to characterize photon energy and fluence distribution independently from one another. Particularly, one would have to decrease the uncertainty of the XFEL photon energy to less than 1 eV.

In addition, there is room for improvement in the theoretical model. Regarding the lasing effect in a dense medium [27,65], which is not considered in our calculations, amplified $K\alpha$ light can induce more valence ionization, thereby reducing the uplift of the +2 peak because increased valence ionization enhances the P-V-F and V-SO-R_{2p}-F pathways, but suppresses the R_{np} -A- R_{2p} -F process, where A competes with V in Ne $1s^{-1}np$. Furthermore, the ions produced by linearly polarized x rays are, to some degree, aligned along the x-ray polarization axis. The resulting anisotropy in the angular distribution of x-ray emission [66] was neglected in our calculations, which may be another source of the discrepancy with experiment. Shakeoff processes are not accurately treated in our model. Moveover, shakeup processes after valence photoionization [67,68] can potentially contribute to a higher population of Ne⁺2 $p^{-1}2\ell^{-1}np$ without a precursor $1s \rightarrow np$ excitation, thus providing more +2 signal at lower photon energy. We also note the limitations of the rateequation approach that we employed. For a better description of resonant x-ray multiphoton physics, one would have to solve density-matrix equations of motion [4,69–71], which capture coherence effects among the pathways leading to the same fluorescing states. Then, we would also expect to see an influence of the pulse-to-pulse fluctuations characteristic of SASE-FEL radiation [72].

Finally, we demonstrate explicitly the role played by the XFEL spectral bandwidth in the pseudoresonance phenomenon. Theoretical data plotted in Fig. 4 illustrate how the fluorescence signals for the ion-core charges of +1 and +2 are affected when decreasing the bandwidth from 1.5% to 0.1% FWHM. Figure 4(a) demonstrates that the pseudoresonance peak gradually disappears as the bandwidth is reduced. At the smallest bandwidth employed in our calculations (0.1%), one can see a weak $1s \rightarrow 2p$ transition located at $E_x \sim 855 \, \text{eV}$, which is dominated by the V–SO– R_{2p} –F pathway. This is not a pseudoresonance, but fully reflects the resonant absorption by Ne^{2+} via the R_{2n} process. Since in a sample of neutral neon atoms, this resonance can only emerge after Ne²⁺ production via an XFEL-induced double-valence-ionization process, such as V–SO, the resonance feature at \sim 855 eV in Fig. 4(a) represents a "hidden resonance." This is an analog of the previously uncovered hidden resonance in the $Q_{ic} = +1$ channel at $E_x = 849 \,\mathrm{eV}$ [4]. In the current study, the latter emerges at spectral bandwidths below 1%, as may be seen in the inset in Fig. 4(b).



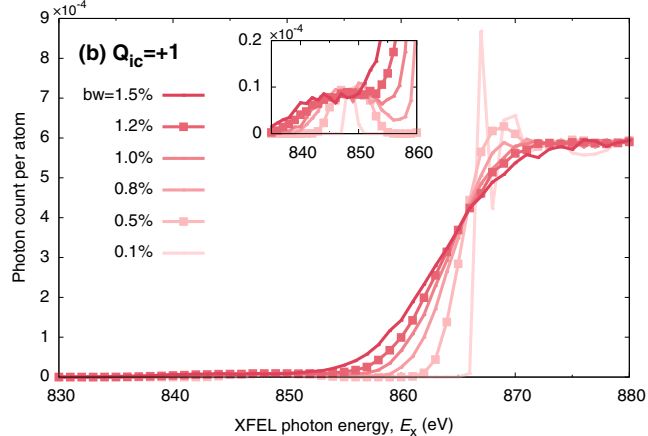


FIG. 4. Theoretical prediction of the XFEL bandwidth dependence of the fluorescence counts for (a) the ion-core charge of +2 and (b) the ion-core charge of +1. The bandwidth (bw) is given in FWHM. Note that the range of XFEL photon energies is extended to a lower energy than shown in Fig. 2 to include the hidden resonance [4] around 849 eV.

In this Letter, we presented a study of multi-RIXS spectroscopy of neon with ultraintense x-ray pulses generated by the European XFEL. We observed an emergent peak that does not match any known resonance position. Through detailed atomic structure and quantum-state-resolved dynamics calculations, we identified the mechanism giving rise to this pseudoresonance. We expect that the pseudoresonance phenomenon uncovered in this work is a general feature, not only for atomic systems but also for complex materials such as molecules, clusters, or solids, whenever two or more sequential resonant photoabsorption events are needed to produce the signal observed and Gaussian broadening dominates the spectral profiles of the resonances involved. As a consequence of the relatively large spectral bandwidth of nonmonochromatized XFEL radiation, resonance-like peaks in XFEL-based absorption spectra do not always represent actual resonances. Our results also demonstrate that this pseudoresonance feature can be controlled by tuning the XFEL bandwidth. Thus, this work provides critical guidance for interpreting data obtained in high-intensity RIXS experiments in which little or no monochromatization is employed to fully exploit the full x-ray fluence provided by XFELs.

Acknowledgments. We acknowledge European XFEL in Schenefeld, Germany, for the provision of x-ray free-electron laser beamtime at SQS (SASE3) under Proposal No. 2954 and would like to thank the staff for their assistance. The construction and implementation of the 1D-imaging soft x-ray spectrometer have been facilitated by an agreement between Uppsala University, European XFEL, and the Swedish Research Council. The support via the VR Grants No. 2012-00114 and No. 2014-06372 is gratefully acknowledged. M.A. acknowledges SSF, Swedish Foundation for Strategic Research, Grant No. RIF14-0064. J.-E.R. acknowledges further support from the Swedish Research Council (Grants No. 2018-04088 and No. 2021-04017). S.-K.S., L.B., C.C., N.R., and R.S. acknowledge support

from DESY, a member of the Helmholtz Association HGF. L.B. and R.S. acknowledge support from DASHH (Data Science in Hamburg - HELMHOLTZ Graduate School for the Structure of Matter) with Grant No. HIDSS-0002. C.C. acknowledges support from the Swedish Research Council (Grants No. 2018-00740 and No. 2021-05988). S.C. and N.T. thank the Swedish Research Council (Grant No. 2019-03935) for financial support. H.A. acknowledges support from the Swedish Research Council on Contract No. 2022-03405. O.B. acknowledges support from Swedish Research Council (Grant No. 2023-1026). A.E.G. acknowledges funding from the European Union Marie Curie Project No. 101067645. I.I. and M.S. acknowledge the CNRS GOtoXFEL program. E.L. acknowledges support from the Swedish Research Council (Grant No. 2020-03315). G.D., K.L., and L.Y. acknowledge support from the U.S. Department of Energy, Office of Science, Basic Energy Science, Chemical Sciences, Geosciences and Biosciences Division under Contract No. DE-AC02-06CH11357. S.C. and J.P. acknowledge support from the Novo Nordisk Foundation Data Science Research Infrastructure 2022 Grant: A high-performance computing infrastructure for data-driven research on sustainable energy materials, Grant No. NNF22OC0078009. J.P. and S.C. also acknowledge financial support from the Technical University of Denmark within the Ph.D. Alliance Programme. M.P. acknowledges Research Council of Finland PROFI5 funding (Grant No. 326291). K.U. acknowledges support from the President's International Fellowship Initiative (PIFI), Grant No. 2021VMA0031. W.X. acknowledges support from the National Natural Science Foundation of China under Grant No. 12174259. This work was supported, in part, by Deutsche Forschungsgemeinschaft (DFG, German Research Foundation) Grant No. 491245950.

Data availability. Some of the data that support the findings of this article are openly available [73], embargo periods may apply. All data shown in tables are available within the article.

Lasers, edited by E. Jaeschke, S. Khan, J. R. Schneider, and J. B. Hastings (Springer, Cham, Switzerland, 2016), pp. 1233–1260.

^[1] R. Santra and L. Young, Interaction of intense x-ray beams with atoms, in *Synchrotron Light Sources and Free-Electron*

- [2] L. Young, E. P. Kanter, B. Krässig, Y. Li, A. M. March, S. T. Pratt, R. Santra, S. H. Southworth, N. Rohringer, L. F. DiMauro, G. Doumy, C. A. Roedig, N. Berrah, L. Fang, M. Hoener, P. H. Bucksbaum, J. P. Cryan, S. Ghimire, J. M. Glownia, D. A. Reis et al., Femtosecond electronic response of atoms to ultra-intense x-rays, Nature (London) 466, 56 (2010).
- [3] M. Hoener, L. Fang, O. Kornilov, O. Gessner, S. T. Pratt, M. Gühr, E. P. Kanter, C. Blaga, C. Bostedt, J. D. Bozek, P. H. Bucksbaum, C. Buth, M. Chen, R. Coffee, J. Cryan, L. Di-Mauro, M. Glownia, E. Hosler, E. Kukk, S. R. Leone *et al.*, Ultraintense x-ray induced ionization, dissociation, and frustrated absorption in molecular nitrogen, Phys. Rev. Lett. 104, 253002 (2010).
- [4] E. P. Kanter, B. Krässig, Y. Li, A. M. March, P. Ho, N. Rohringer, R. Santra, S. H. Southworth, L. F. DiMauro, G. Doumy, C. A. Roedig, N. Berrah, L. Fang, M. Hoener, P. H. Bucksbaum, S. Ghimire, D. A. Reis, J. D. Bozek, C. Bostedt, M. Messerschmidt *et al.*, Unveiling and driving hidden resonances with high-fluence, high-intensity x-ray pulses, Phys. Rev. Lett. 107, 233001 (2011).
- [5] G. Doumy, C. Roedig, S.-K. Son, C. I. Blaga, A. D. DiChiara, R. Santra, N. Berrah, C. Bostedt, J. D. Bozek, P. H. Bucksbaum, J. P. Cryan, L. Fang, S. Ghimire, J. M. Glownia, M. Hoener, E. P. Kanter, B. Krässig, M. Kuebel, M. Messerschmidt, G. G. Paulus *et al.*, Nonlinear atomic response to intense ultrashort x rays, Phys. Rev. Lett. **106**, 083002 (2011).
- [6] L. Fang, T. Osipov, B. Murphy, F. Tarantelli, E. Kukk, J. P. Cryan, M. Glownia, P. H. Bucksbaum, R. N. Coffee, M. Chen, C. Buth, and N. Berrah, Multiphoton ionization as a clock to reveal molecular dynamics with intense short x-ray free electron laser pulses, Phys. Rev. Lett. 109, 263001 (2012).
- [7] B. Rudek, S.-K. Son, L. Foucar, S. W. Epp, B. Erk, R. Hartmann, M. Adolph, R. Andritschke, A. Aquila, N. Berrah, C. Bostedt, J. Bozek, N. Coppola, F. Filsinger, H. Gorke, T. Gorkhover, H. Graafsma, L. Gumprecht, A. Hartmann, G. Hauser *et al.*, Ultra-efficient ionization of heavy atoms by intense x-ray free-electron laser pulses, Nat. Photon. 6, 858 (2012).
- [8] H. Fukuzawa, S.-K. Son, K. Motomura, S. Mondal, K. Nagaya, S. Wada, X.-J. Liu, R. Feifel, T. Tachibana, Y. Ito, M. Kimura, T. Sakai, K. Matsunami, H. Hayashita, J. Kajikawa, P. Johnsson, M. Siano, E. Kukk, B. Rudek, B. Erk *et al.*, Deep inner-shell multiphoton ionization by intense x-ray free-electron laser pulses, Phys. Rev. Lett. 110, 173005 (2013).
- [9] B. F. Murphy, T. Osipov, Z. Jurek, L. Fang, S.-K. Son, M. Mucke, J. H. D. Eland, V. Zhaunerchyk, R. Feifel, L. Avaldi, P. Bolognesi, C. Bostedt, J. D. Bozek, J. Grilj, M. Guehr, L. J. Frasinski, J. Glownia, D. T. Ha, K. Hoffmann, E. Kukk *et al.*, Femtosecond x-ray-induced explosion of C₆₀ at extreme intensity, Nat. Commun. 5, 4281 (2014).
- [10] B. Rudek, K. Toyota, L. Foucar, B. Erk, R. Boll, C. Bomme, J. Correa, S. Carron, S. Boutet, G. J. Williams, K. R. Ferguson, R. Alonso-Mori, J. E. Koglin, T. Gorkhover, M. Bucher, C. S. Lehmann, B. Krässig, S. H. Southworth, L. Young, C. Bostedt et al., Relativistic and resonant effects in the ionization of heavy atoms by ultra-intense hard x-rays, Nat. Commun. 9, 4200 (2018).
- [11] N. Berrah, A. Sanchez-Gonzalez, Z. Jurek, R. Obaid, H. Xiong, R. J. Squibb, T. Osipov, A. Lutman, L. Fang, T. Barillot, J. D. Bozek, J. Cryan, T. J. A. Wolf, D. Rolles, R. Coffee, K.

- Schnorr, S. Augustin, H. Fukuzawa, K. Motomura, N. Niebuhr *et al.*, Femtosecond-resolved observation of the fragmentation of buckminsterfullerene following x-ray multiphoton ionization, Nat. Phys. **15**, 1279 (2019).
- [12] A. C. LaForge, S.-K. Son, D. Mishra, M. Ilchen, S. Duncanson, E. Eronen, E. Kukk, S. Wirok-Stoletow, D. Kolbasova, P. Walter, R. Boll, A. D. Fanis, M. Meyer, Y. Ovcharenko, D. E. Rivas, P. Schmidt, S. Usenko, R. Santra, and N. Berrah, Resonanceenhanced multiphoton ionization in the x-ray regime, Phys. Rev. Lett. 127, 213202 (2021).
- [13] A. Rörig, S.-K. Son, T. Mazza, P. Schmidt, T. M. Baumann, B. Erk, M. Ilchen, J. Laksman, V. Music, S. Pathak, D. E. Rivas, D. Rolles, S. Serkez, S. Usenko, R. Santra, M. Meyer, and R. Boll, Multiple-core-hole resonance spectroscopy with ultraintense x-ray pulses, Nat. Commun. 14, 5738 (2023).
- [14] N. Berrah, L. Fang, B. Murphy, T. Osipov, K. Ueda, E. Kukk, R. Feifel, P. van der Meulen, P. Salen, H. T. Schmidt, R. D. Thomas, M. Larsson, R. Richter, K. C. Prince, J. D. Bozek, C. Bostedt, S.-I. Wada, M. N. Piancastelli, M. Tashiro, and M. Ehara, Double-core-hole spectroscopy for chemical analysis with an intense x-ray femtosecond laser, Proc. Natl. Acad. Sci. USA 108, 16912 (2011).
- [15] T. Tachibana, Z. Jurek, H. Fukuzawa, K. Motomura, K. Nagaya, S. ichi Wada, P. Johnsson, M. Siano, S. Mondal, Y. Ito, M. Kimura, T. Sakai, K. Matsunami, H. Hayashita, J. Kajikawa, X.-J. Liu, E. Robert, C. Miron, R. Feifel, J. P. Marangos *et al.*, Nanoplasma formation by high intensity hard x-rays, Sci. Rep. 5, 10977 (2015).
- [16] Y. Kumagai, Z. Jurek, W. Xu, H. Fukuzawa, K. Motomura, D. Iablonskyi, K. Nagaya, S. ichi Wada, S. Mondal, T. Tachibana, Y. Ito, T. Sakai, K. Matsunami, T. Nishiyama, T. Umemoto, C. Nicolas, C. Miron, T. Togashi, K. Ogawa, S. Owada *et al.*, Radiation-induced chemical dynamics in Ar clusters exposed to strong x-ray pulses, Phys. Rev. Lett. 120, 223201 (2018).
- [17] T. Mazza, M. Ilchen, M. D. Kiselev, E. V. Gryzlova, T. M. Baumann, R. Boll, A. De Fanis, P. Grychtol, J. Montaño, V. Music, Y. Ovcharenko, N. Rennhack, D. E. Rivas, P. Schmidt, R. Wagner, P. Ziolkowski, N. Berrah, B. Erk, P. Johnsson, C. Küstner-Wetekam *et al.*, Mapping resonance structures in transient core-ionized atoms, Phys. Rev. X 10, 041056 (2020).
- [18] B. I. Cho, K. Engelhorn, S. M. Vinko, H.-K. Chung, O. Ciricosta, D. S. Rackstraw, R. W. Falcone, C. R. D. Brown, T. Burian, J. Chalupský, C. Graves, V. Hájková, A. Higginbotham, L. Juha, J. Krzywinski, H. J. Lee, M. Messersmidt, C. Murphy, Y. Ping, N. Rohringer *et al.*, Resonant *Kα* spectroscopy of solid-density aluminum plasmas, Phys. Rev. Lett. 109, 245003 (2012).
- [19] S. M. Vinko, O. Ciricosta, B. I. Cho, K. Engelhorn, H.-K. Chung, C. R. D. Brown, T. Burian, J. Chalupský, R. W. Falcone, C. Graves, V. Hájková, A. Higginbotham, L. Juha, J. Krzywinski, H. J. Lee, M. Messerschmidt, C. D. Murphy, Y. Ping, A. Scherz, W. Schlotter *et al.*, Creation and diagnosis of a solid-density plasma with an x-ray free-electron laser, Nature (London) 482, 59 (2012).
- [20] R. Obaid, C. Buth, G. L. Dakovski, R. Beerwerth, M. Holmes, J. Aldrich, M.-F. Lin, M. Minitti, T. Osipov, and W. Schlotter, LCLS in—photon out: Fluorescence measurement of neon using soft x-rays, J. Phys. B: At. Mol. Opt. Phys. 51, 034003 (2018).

- [21] K. Tamasaku, M. Nagasono, H. Iwayama, E. Shigemasa, Y. Inubushi, T. Tanaka, K. Tono, T. Togashi, T. Sato, T. Katayama, T. Kameshima, T. Hatsui, M. Yabashi, and T. Ishikawa, Double core-hole creation by sequential attosecond photoionization, Phys. Rev. Lett. 111, 043001 (2013).
- [22] F. Gel'mukhanov, M. Odelius, S. P. Polyutov, A. Föhlisch, and V. Kimberg, Dynamics of resonant x-ray and auger scattering, Rev. Mod. Phys. 93, 035001 (2021).
- [23] C. Pellegrini, A. Marinelli, and S. Reiche, The physics of x-ray free-electron lasers, Rev. Mod. Phys. 88, 015006 (2016).
- [24] E. A. Seddon, J. A. Clarke, D. J. Dunning, C. Masciovecchio, C. J. Milne, F. Parmigiani, D. Rugg, J. C. H. Spence, N. R. Thompson, K. Ueda, S. M. Vinko, J. S. Wark, and W. Wurth, Short-wavelength free-electron laser sources and science: A review, Rep. Prog. Phys. 80, 115901 (2017).
- [25] M. Beye, P. Wernet, C. Schüßler-Langeheine, and A. Föhlisch, Time resolved resonant inelastic x-ray scattering: A supreme tool to understand dynamics in solids and molecules, J. Electron Spectrosc. Relat. Phenom. 188, 172 (2013).
- [26] N. Rohringer, X-ray Raman scattering: A building block for nonlinear spectroscopy, Phil. Trans. R. Soc. A. 377, 20170471 (2019).
- [27] C. Weninger, M. Purvis, D. Ryan, R. A. London, J. D. Bozek, C. Bostedt, A. Graf, G. Brown, J. J. Rocca, and N. Rohringer, Stimulated electronic x-ray Raman scattering, Phys. Rev. Lett. 111, 233902 (2013).
- [28] V. Kimberg, A. Sanchez-Gonzalez, L. Mercadier, C. Weninger, A. Lutman, D. Ratner, R. Coffee, M. Bucher, M. Mucke, M. Agåker, C. Såthe, C. Bostedt, J. Nordgren, J. E. Rubensson, and N. Rohringer, Stimulated x-ray Raman scattering – a critical assessment of the building block of nonlinear x-ray spectroscopy, Faraday Discuss. 194, 305 (2016).
- [29] U. Eichmann, H. Rottke, S. Meise, J.-E. Rubensson, J. Söderström, M. Agåker, C. Såthe, M. Meyer, T. M. Baumann, R. Boll, A. De Fanis, P. Grychtol, M. Ilchen, T. Mazza, J. Montano, V. Music, Y. Ovcharenko, D. E. Rivas, S. Serkez, R. Wagner *et al.*, Photon-recoil imaging: Expanding the view of nonlinear x-ray physics, Science 369, 1630 (2020).
- [30] K. Li, C. Ott, M. Agåker, P. J. Ho, G. Doumy, A. Magunia, M. Rebholz, M. Simon, T. Mazza, A. D. Fanis, T. M. Baumann, J. Montano, N. Rennhack, S. Usenko, Y. Ovcharenko, K. Chordiya, L. Cheng, J.-E. Rubensson, M. Meyer, T. Pfeifer et al., Super-resolution stimulated x-ray Raman spectroscopy, Nature (London) 643, 662 (2025).
- [31] S. Mukamel, D. Healion, Y. Zhang, and J. D. Biggs, Multidimensional attosecond resonant x-ray spectroscopy of molecules: Lessons from the optical regime, Annu. Rev. Phys. Chem. **64**, 101 (2013).
- [32] A. S. Morillo-Candas, S. M. Augustin, E. Prat, A. Sarracini, J. Knurr, S. Zerdane, Z. Sun, N. Yang, M. Rebholz, H. Zhang, Y. Deng, X. Xie, A. Cannizzo, A. Al-Haddad, K. A. Schnorr, C. Ott, T. Feurer, C. Bostedt, T. Pfeifer, and G. Knopp, Coherent all x-ray four wave mixing at core shell resonances, arXiv:2408.11881 (2024).
- [33] P. Wernet, K. Kunnus, I. Josefsson, I. Rajkovic, W. Quevedo, M. Beye, S. Schreck, S. Grübel, M. Scholz, D. Nordlund, W. Zhang, R. W. Hartsock, W. F. Schlotter, J. J. Turner, B. Kennedy, F. Hennies, F. M. F. de Groot, K. J. Gaffney, S. Techert, M. Odelius et al., Orbital-specific mapping of the

- ligand exchange dynamics of Fe(CO)₅ in solution, Nature (London) **520**, 78 (2015).
- [34] T. Marchenko, S. Carniato, L. Journel, R. Guillemin, E. Kawerk, M. Žitnik, M. Kavčič, K. Bučar, R. Bohinc, M. Petric, V. Vaz da Cruz, F. Gel'mukhanov, and M. Simon, Electron dynamics in the core-excited CS₂ molecule revealed through resonant inelastic x-ray scattering spectroscopy, Phys. Rev. X 5, 031021 (2015).
- [35] L. Kjellsson, K. D. Nanda, J.-E. Rubensson, G. Doumy, S. H. Southworth, P. J. Ho, A. M. March, A. Al Haddad, Y. Kumagai, M.-F. Tu, R. D. Schaller, T. Debnath, M. S. Bin Mohd Yusof, C. Arnold, W. F. Schlotter, S. Moeller, G. Coslovich, J. D. Koralek, M. P. Minitti, M. L. Vidal *et al.*, Resonant inelastic x-ray scattering reveals hidden local transitions of the aqueous oh radical, Phys. Rev. Lett. 124, 236001 (2020).
- [36] O. S. Humphries, R. S. Marjoribanks, Q. Y. van den Berg, E. C. Galtier, M. F. Kasim, H. J. Lee, A. J. F. Miscampbell, B. Nagler, R. Royle, J. S. Wark, and S. M. Vinko, Probing the electronic structure of warm dense nickel via resonant inelastic x-ray scattering, Phys. Rev. Lett. 125, 195001 (2020).
- [37] K. Tamasaku, M. Taguchi, I. Inoue, T. Osaka, Y. Inubushi, M. Yabashi, and T. Ishikawa, Two-dimensional $K\beta K\alpha$ fluorescence spectrum by nonlinear resonant inelastic x-ray scattering, Nat. Commun. 14, 4262 (2023).
- [38] A. Forte, T. Gawne, K. K. A. El-Din, O. S. Humphries, T. R. Preston, C. Crépisson, T. Campbell, P. Svensson, S. Azadi, P. Heighway, Y. Shi, D. A. Chin, E. Smith, C. Baehtz, V. Bouffetier, H. Höppner, D. McGonegle, M. Harmand, G. W. Collins, J. S. Wark *et al.*, Resonant inelastic x-ray scattering in warm-dense fe compounds beyond the SASE FEL resolution limit, Commun. Phys. 7, 266 (2024).
- [39] B. Rudek, D. Rolles, S.-K. Son, L. Foucar, B. Erk, S. Epp, R. Boll, D. Anielski, C. Bostedt, S. Schorb, R. Coffee, J. Bozek, S. Trippel, T. Marchenko, M. Simon, L. Christensen, S. De, S.-I. Wada, K. Ueda, I. Schlichting *et al.*, Resonance-enhanced multiple ionization of krypton at an x-ray free-electron laser, Phys. Rev. A 87, 023413 (2013).
- [40] P. J. Ho, C. Bostedt, S. Schorb, and L. Young, Theoretical tracking of resonance-enhanced multiple ionization pathways in x-ray free-electron laser pulses, Phys. Rev. Lett. 113, 253001 (2014).
- [41] K. Toyota, S.-K. Son, and R. Santra, Interplay between relativistic energy corrections and resonant excitations in x-ray multiphoton ionization dynamics of xe atoms, Phys. Rev. A 95, 043412 (2017).
- [42] T. M. Baumann, S.-K. Son, J.-E. Rubensson *et al.* (unpublished).
- [43] J. Schlappa, G. Ghiringhelli, B. E. Van Kuiken, M. Teichmann, P. S. Miedema, J. T. Delitz, N. Gerasimova, S. Molodtsov, L. Adriano, B. Baranasic, C. Broers, R. Carley, P. Gessler, N. Ghodrati, D. Hickin, L. P. Hoang, M. Izquierdo, L. Mercadier, G. Mercurio, S. Parchenko *et al.*, The heisenberg-rixs instrument at the european XFEL, J. Synchrotron Radiat. 32, 29 (2025).
- [44] N. Gerasimova, D. La Civita, L. Samoylova, M. Vannoni, R. Villanueva, D. Hickin, R. Carley, R. Gort, B. E. Van Kuiken, P. Miedema, L. Le Guyarder, L. Mercadier, G. Mercurio, J. Schlappa, M. Teichman, A. Yaroslavtsev, H. Sinn, and A. Scherz, The soft x-ray monochromator at the SASE3

- beamline of the european XFEL: From design to operation, J. Synchrotron Radiat. **29**, 1299 (2022).
- [45] W. Decking *et al.*, A MHz-repetition-rate hard x-ray free-electron laser driven by a superconducting linear accelerator, Nat. Photon. **14**, 391 (2020).
- [46] M. Agåker, J. Söderström, T. M. Baumann, C.-J. Englund, L. Kjellsson, R. Boll, A. De Fanis, S. Dold, T. Mazza, J. Montaño, A. Münnich, T. Mullins, Y. Ovcharenko, N. Rennhack, P. Schmidt, B. Senfftleben, M. Turcato, S. Usenko, M. Meyer, J. Nordgren *et al.*, A 1D imaging soft x-ray spectrometer for the small quantum systems instrument at european XFEL, J. Synchrotron Radiat. 31, 1264 (2024).
- [47] T. Tschentscher, C. Bressler, J. Grünert, A. Madsen, A. P. Mancuso, M. Meyer, A. Scherz, H. Sinn, and U. Zastrau, Photon beam transport and scientific instruments at the european XFEL, Appl. Sci. 7, 592 (2017).
- [48] See Supplemental Material at http://link.aps.org/supplemental/ 10.1103/drmh-vmgk for detailed calibration and calculation procedures and dependence on XFEL beam parameters.
- [49] H. Ågren, J. Nordgren, L. Selander, C. Nordling, and K. Siegbahn, Multiplet structure in the high-resolution x-ray emission spectrum of neon, J. Electron Spectrosc. Relat. Phenom. **14**, 27 (1978).
- [50] M. Oura, Study of inner-shell excitation and relaxation processes in atomic and ionic neon by means of soft x-ray spectroscopy, Plasma Sci. Technol. 12, 353 (2010).
- [51] A. Müller, D. Bernhardt, A. Borovik, T. Buhr, J. Hellhund, K. Holste, A. L. D. Kilcoyne, S. Klumpp, M. Martins, S. Ricz, J. Seltmann, J. Viefhaus, and S. Schippers, Photoionization of ne atoms and Ne⁺ ions near the K edge: Precision spectroscopy and absolute cross-sections, Astrophys. J. 836, 166 (2017).
- [52] A. Picón, J. Mompart, and S. H. Southworth, Stimulated Raman adiabatic passage with two-color x-ray pulses, New J. Phys. 17, 083038 (2015).
- [53] K. Anderson, P. A. Malmqvist, and B. O. Roos, Second-order perturbation theory with a complete active space self-consistent field reference function, J. Chem. Phys. 96, 1218 (1992).
- [54] J. Finley, P.-Å. Malmqvist, B. O. Roos, and L. Serrano-Andrés, The multi-state CASPT2 method, Chem. Phys. Lett. 288, 299 (1998).
- [55] J. Olsen, B. O. Roos, P. Jørgensen, and H. J. A. Jensen, Determinant based configuration interaction algorithms for complete and restricted configuration interaction spaces, J. Chem. Phys. 89, 2185 (1988).
- [56] V. Sauri, L. Serrano-Andrés, A. R. M. Shahi, L. Gagliardi, S. Vancoillie, and K. Pierloot, Multiconfigurational second-order perturbation theory restricted active space (RASPT2) method for electronic excited states: A benchmark study, J. Chem. Theory Comput. 7, 153 (2011).
- [57] G. Li Manni, I. Fdez. Galván, A. Alavi, F. Aleotti, F. Aquilante, J. Autschbach, D. Avagliano, A. Baiardi, J. J. Bao, S. Battaglia, L. Birnoschi, A. Blanco-González, S. I. Bokarev, R. Broer, R. Cacciari, P. B. Calio, R. K. Carlson, R. Carvalho Couto,

- L. Cerdán, L. F. Chibotaru *et al.*, The OpenMolcas web: A community-driven approach to advancing computational chemistry, J. Chem. Theory Comput. **19**, 6933 (2023).
- [58] S.-K. Son, L. Young, and R. Santra, Impact of hollow-atom formation on coherent x-ray scattering at high intensity, Phys. Rev. A **83**, 033402 (2011).
- [59] L. Budewig, S.-K. Son, and R. Santra, Theoretical investigation of orbital alignment of x-ray-ionized atoms in exotic electronic configurations, Phys. Rev. A **105**, 033111 (2022).
- [60] L. Budewig, S.-K. Son, and R. Santra, State-resolved ionization dynamics of a neon atom induced by x-ray free-electron-laser pulses, Phys. Rev. A **107**, 013102 (2023).
- [61] S. L. Carter and H. P. Kelly, Double photoionization of neon and argon, Phys. Rev. A 16, 1525 (1977).
- [62] N. Saito and I. H. Suzuki, Shake-off processes in photoionization and auger transition for rare gases irradiated by soft x-rays, Phys. Scr. **49**, 80 (1994).
- [63] K. Toyota, Z. Jurek, S.-K. Son, H. Fukuzawa, K. Ueda, N. Berrah, B. Rudek, D. Rolles, A. Rudenko, and R. Santra, *xcalib*: A focal spot calibrator for intense x-ray free-electron laser pulses based on the charge state distributions of light atoms, J. Synchrotron Radiat. 26, 1017 (2019).
- [64] N. Breckwoldt, S.-K. Son, T. Mazza, A. Rörig, R. Boll, M. Meyer, A. C. LaForge, D. Mishra, N. Berrah, and R. Santra, Machine-learning calibration of intense x-ray free-electron-laser pulses using Bayesian optimization, Phys. Rev. Res. 5, 023114 (2023).
- [65] C. Weninger and N. Rohringer, Stimulated resonant x-ray Raman scattering with incoherent radiation, Phys. Rev. A 88, 053421 (2013).
- [66] H. Schmoranzer, S. Lauer, F. Vollweiler, A. Ehresmann, V. L. Sukhorukov, B. M. Lagutin, I. D. Petrov, P. V. Demekhin, K.-H. Schartner, B. Magel, and G. Mentzel, Angular distribution of the fluorescence radiation of Kr II satellite states, J. Phys. B: At. Mol. Opt. Phys. 30, 4463 (1997).
- [67] A. Kikas, S. J. Osborne, A. Ausmees, S. Svensson, O.-P. Sairanen, and S. Aksela, High-resolution study of the correlation satellites in photoelectron spectra of the rare gases, J. Electron Spectrosc. Relat. Phenom. 77, 241 (1996).
- [68] N. Watanabe and M. Takahashi, Revisiting electron-correlation effects on valence shake-up satellites of neon, Phys. Rev. A 100, 032710 (2019).
- [69] N. Rohringer and R. Santra, Strongly driven resonant auger effect treated by an open-quantum-system approach, Phys. Rev. A 86, 043434 (2012).
- [70] S. M. Cavaletto, C. Buth, Z. Harman, E. P. Kanter, S. H. Southworth, L. Young, and C. H. Keitel, Resonance fluorescence in ultrafast and intense x-ray free-electron-laser pulses, Phys. Rev. A 86, 033402 (2012).
- [71] Y. Li, C. Gao, W. Dong, J. Zeng, Z. Zhao, and J. Yuan, Coherence and resonance effects in the ultra-intense laser-induced ultrafast response of complex atoms, Sci. Rep. 6, 18529 (2016).
- [72] N. Rohringer and R. Santra, X-ray nonlinear optical processes using a self-amplified spontaneous emission free-electron laser, Phys. Rev. A **76**, 033416 (2007).
- [73] https://doi.org/10.22003/XFEL.EU-DATA-002954-00.